Practical Position and Yaw Rate Estimation with GPS and Differential Wheelspeeds

Christopher R. Carlson
Stanford University
Mechanical Engineering
Stanford, CA 94305-4021, USA
crcarlson@stanford.edu

J. Christian Gerdes
Stanford University
Mechanical Engineering
Stanford, CA 94305-4021, USA
gerdes@cdr.stanford.edu

J. David Powell
Stanford University
Aeronautics & Astronautics
Stanford, CA 94305-4035, USA
jdpowell@stanford.edu

This paper compares two different global position estimation strategies for vehicle navigation. Both estimate individual wheel radii with GPS and then use wheelspeed information to estimate the path length travelled. One further uses wheelspeed information to estimate vehicle heading. The other uses GPS to calibrate the bias and scale factor of an automotive grade gyroscope which is then used to estimate vehicle heading. Detailed model assumptions are discussed including the error contributions of several modeling simplifications. Test results show the gyro and wheelspeed-heading schemes perform equally when modeling assumptions hold, such as when navigating smooth road surfaces. However, the wheelspeed-heading estimator exhibits more sensitivity to wheel slip and road surface. Its position errors grow about twice as fast when the vehicle navigates speed bumps and uneven road surfaces. Increasing the resolution of the stock wheelspeed sensors does not increase the positioning accuracy of either estimator. Both schemes may benefit by compensating for wheel slip during braking.

Keywords/ GPS, navigation, odometer, noise model, vehicle dynamics, gyro bias, gyro scale factor

1 INTRODUCTION

Current automotive navigation systems such as those proposed in [1, 8, 11, 12, 17] estimate vehicle position using some combination of Global Positioning System (GPS), odometer, and heading sensors. Each of the authors discuss advantages of estimating sensor biases by blending inertial sensors with GPS in some form of Kalman filter (KF). Abbott [1] thoroughly quantifies which sensors contribute the most uncertainty to the position solution. In all cases, the inertial measurements offer little correction to the GPS position solutions and are primarily used during periods of GPS unavailability.

GPS is a line of sight sensor technology which needs at least 4 satellites in view to form a unique position solution [8, 10]. When navigating areas with limited sky visibility a navigation system must rely on integrating its inertial sensors to estimate vehicle position. Such situations include: between tall buildings; underneath trees; inside parking structures; and under bridges.

This paper investigates how differential wheelspeed sensors from the factory installed Antilock Braking System (ABS) may be used to estimate heading during periods of GPS unavailability. Stephen [17] first attempted this using the frequency of the undriven wheel pulse trains to estimate wheel angular velocity. He then switched to counting the zero crossings of each pulse train. In each case the rear wheel radii were estimated by taking the ratio of GPS velocity to the estimate of wheel angular velocity. The radius estimates are then individually low-pass filtered with a long time constants to reduce the effect of the velocity disturbances at the rear wheels due to yaw rate (This disturbance will be explained in more detail in Section 2.) Rogers [11] uses a similar heading estimation technique with dual ground radar sensors in place of wheelspeeds. In [12] the same author uses external wheel encoders to form a wheelspeed based dead-reckoning system.

This paper expands on these ideas to include the independent wheel radii in an Extended Kalman Filter (EKF) structure. Doing so takes advantage of the kinematic coupling of vehicle yaw rate at each wheel. Other navigation systems with an explicit heading sensor, such as a magnetic compass or yaw gyro, model the rear wheels with a single effective radius [1, 8, 11]. This is a good model when the rear wheel radii are the same, but section 5 shows it can lead to large errors when tire radii which differ by more than $5[cm]$ such as when navigating with a spare tire.

This paper also discusses the potential benefits of calculated GPS antennae placement. A kinematic analysis shows that placing the antenna along the centerline of the vehicle over the rear differential should minimize a vehicle sideslip dependent bias. Section 2.2 includes an error analysis which describes the error produced by placing the antenna over the CG of the test vehicle.

The errors induced by quantizing a signal are commonly modeled as white noise sequences [1, 8]. Section 3 discusses a physical explanation and numerical simulation for why this analysis may be overly conservative. Additionally, navigation filters which use quantized wheelspeed measurements implemented in Section 7 consistently estimate heading better than a white noise analysis predicts. Test data

in Section 7.2.3 shows that increasing the resolution of the wheel angle encoder from 100[$ticks/rev$] to 2000[$ticks/rev$] does not improve the dead-reckoning global positioning accuracy by more than 2[cm].

Current gyroscopes have a scale factor and bias which can vary by as much as 2% and drift over the life of the sensor [1]. Systems with existing yaw gyros such as driver assistance systems [6, 13, 18] may benefit by identifying gyro bias and scale factor in real time. This paper proposes and experimentally tests a filter structure which estimates gyro bias and scale factor in addition to vehicle heading and position with GPS and ABS sensors. The results from the gyro based filter also form a nice baseline with which to compare with the wheelspeed heading based filter.

With the introduction of MEMS and other technology to the automotive market, the cost of high quality gyros will almost certainly decrease. As such, redundant vehicle heading and yaw rate estimation from alternate sensors can provide robust models for on board vehicle diagnostics [15].

2 DIFFERENTIAL WHEEL VELOCITIES

Figure 1 shows the kinematic car model used for these applications. V is the velocity at the CG, the

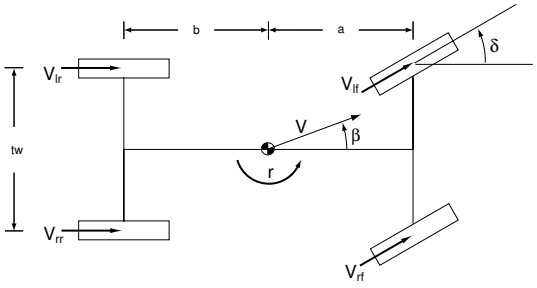

Figure 1: Vehicle model

V_{xx} terms represent the velocities at each wheel, β is the vehicle side slip angle, r is vehicle yaw rate, δ is the steering angle and tw_r is the rear track width of the vehicle. Given this model,

$$V_{lr} = V\cos\beta - \frac{tw_r}{2}r \quad (1)$$

$$V_{rr} = V\cos\beta + \frac{tw_r}{2}r \quad (2)$$

$$\Rightarrow$$

$$r = \frac{V_{rr} - V_{lr}}{tw_r} \quad (3)$$

This equation for yaw rate generated the initial inspiration for the work in this paper. Similarly, the front wheels yield

$$r = \frac{V_{rf} - V_{lf}}{tw_f \cos(\delta)} \quad (4)$$

2.1 Absolute Velocity Reference

One way to calibrate the wheel effective radii is to drive a known distance and divide by the number of revolutions of the tire. Current availability and predicted ubiquity [10] make GPS a practical sensor for absolute positioning, however, without some sort of differential correction the GPS position estimate is usually biased. For this reason the filters in this paper use the ratio of the effectively unbiased [8] GPS velocity and the wheel angular velocity to identify wheel effective radius.

2.2 Assumption: No Sideslip

The vehicle radius estimation scheme in this paper assumes a longitudinal velocity measurement which has no sideslip components adding to the measurement. At low speeds when sideslip is the highest the velocity signal becomes dependent upon antenna position. Figure 2 shows the tire radius estimates for two different antenna positions on a vehicle circling the top of a parking garage (figure 7). The top curves

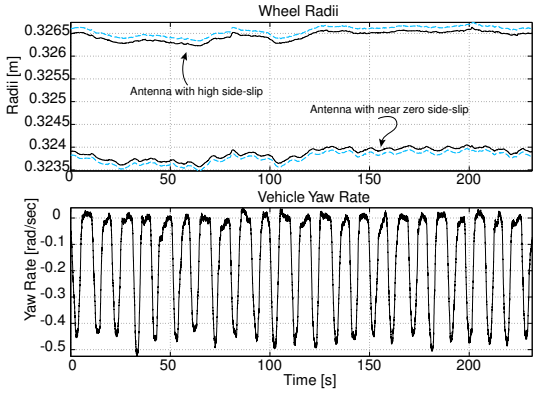

Figure 2: Rear wheel radius estimates for different GPS antenna locations

have the antenna placed over the Center of Gravity (CG), the lower curves have the antennae placed over the rear differential of the vehicle. The difference in radii can be explained by looking at the kinematics of vehicle motion.

Let $\hat{\imath}, \hat{\jmath}$ be the unit vectors in the longitudinal and lateral directions, then the equation for the velocity of the CG

$$V^{CG} = \frac{V_{rr} + V_{rl}}{2}\hat{\imath} + rb\hat{\jmath} \quad (5)$$

shows an additional velocity term due yaw rate times the distance from the CG to the rear axle. At low speeds and high turn rates, this will add a velocity error to the measurement. At higher lateral accelerations the sideslip at the rear tires will be nonzero, however, the lateral velocity component is usually small and should have a small effect.

Assuming the filter with the antenna placed over the CG lost the GPS measurement and continued its INS dead-reckoning from the above results, we would expect the longitudinal error to grow as:

$$e = \int_0^t \frac{\Omega^r \Delta R^r + \Omega^l \Delta R^l}{2} \quad (6)$$

At 10[m/s] this would cause longitudinal error growth of 0.08[m/s]. This translates to a little less than 1% error. Although small, this error could be

easily avoided by placing the antenna over the rear differential. If desired, vehicle sideslip can be estimated with similar equipment to what was used for the navigation work in this paper: GPS and a yaw gyro, see[3, 14].

3 QUANTIZATION & WHITE NOISE

In engineering practice, velocity measurements are frequently estimated by numerically differentiating a discrete position signal. Section 2 presented a model which describes the kinematic relationship between wheel velocities and vehicle yaw rate. For this application, wheel angular velocity $\omega(t)$ at time $k\Delta t$ for small Δt can be approximated as:

$$\omega(k\Delta t) = \omega_k(k) \quad (7)$$

$$\cong \frac{\theta_k - \theta_{k-1}}{\Delta t} \quad (8)$$

Where Δt is the discrete sampling time. If we assume the measurements $\hat{\theta}_k$ are quantized by an encoder signal,

$$\hat{\theta}_k = \theta_k + \delta\theta_k \quad (9)$$

then the errors induced by the quantization at each time step are

$$\epsilon_k(k) = \frac{\delta\theta_k - \delta\theta_{k-1}}{\Delta t} \quad (10)$$

A reasonable question to pose is, how does the sequence of numbers, ϵ_k, behave? Throughout most of this paper, we will find that sequences like $\hat{\omega}_k$ will drive first order difference equations. So, how does the numerical integral of $\hat{\omega}_k$ behave?

Figure 3 shows two signals ω_k and $\hat{\omega}_k$. ω_k represents a $24[rad/s]$ mean angular velocity signal with a $12[rad/s]$ sinusoid added on top of it to simulate clean, smooth velocity variation. These angular velocities for a vehicle tire with radius of $0.3[m]$ correspond to a mean vehicle velocity of $8[m/s]$ with a $4[m/s]$ velocity variation. $\hat{\omega}_k$ is the euler velocity signal quantized at the ABS sensor angle resolution of $100/(2\pi)[ticks/rad]$

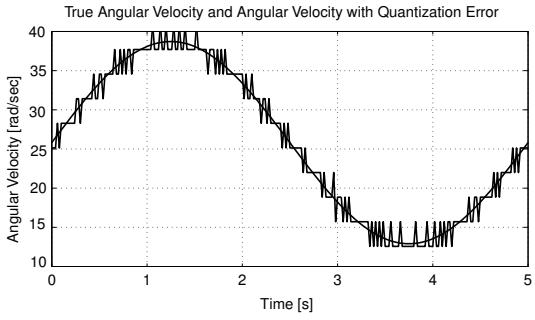

Figure 3: Simulated angular velocity and quantized angular velocity trace

The error between the two signals, ϵ_k, is often approximated as a white noise sequence. Figure 4 shows the qualitative similarity of ϵ_k and a white noise sequence with the same mean and variance.

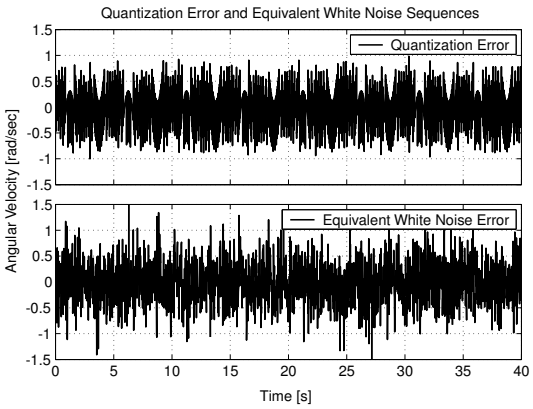

Figure 4: Quantized angular velocity error and equivalent white noise sequence

For a discrete time integrator forced by white noise with covariance R_k and an initial covariance of the state P_0,

$$x_{k+1} = x_k + v_k \quad (11)$$

$$v_k \sim N(0, R_k) \quad (12)$$

$$E(x_0 x_0^T) = P_0 \quad (13)$$

it is well known [5, 16] that the covariance of x(t) can be approximated as:

$$P(k\Delta t) = E(x(k\Delta t)x^T(k\Delta t)) \quad (14)$$

$$\cong P_0 + tR_k\Delta t \quad (15)$$

So the variance of the states grows linearly in time and the rate with which it grows is proportional to the sample rate. This is the classical random walk equation.

Now let q_k represent the position measurement from an encoder and let e_k represent the encoder's quantization noise. Then $\hat{w}_k$ can represent the Euler approximated velocity for encoder signal.

$$\hat{w}_k = \frac{q_k + e_k}{\Delta t} \quad (16)$$

$$\hat{y}_{k+1} = \hat{y}_k + \hat{w}_k\Delta t \quad (17)$$

The difference equation $\hat{y}_k$ now represents the total position measurement of some encoder, and has a much different variance than equation 11. If y_k represents the true position signal, then

$$|\hat{y_k} - y_k| < \max|q_k| \qquad \forall k \quad (18)$$

The errors in w_k are correlated, over time the errors in the new measurements cancel out the errors in the old measurements. The largest error from a quantized, deterministic signal should be within the magnitude of the quantization error. The variance of the state whose differential equation is driven by the "noise" process w_k does not grow in time. Figure 5 shows a MATLAB simulation of the integral of the error signal ω_k, the integral of one instance of a white noise signal with the same variance and the bounding function for the standard deviation of the white noise

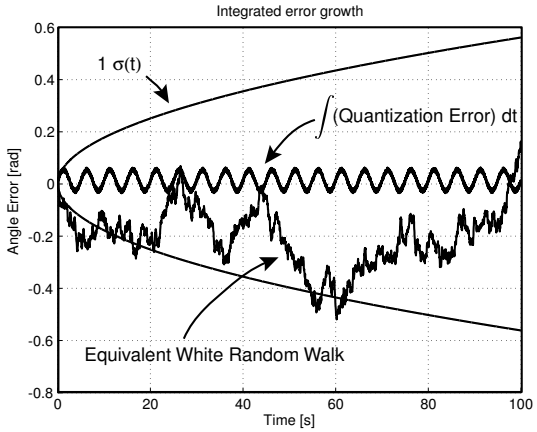

Figure 5: Error growth of integrated quantized velocity and equivalent white noise sequences at 50hz

sequence as described by equation 15. The sinusoidal nature of the quantization error is an artifact of the input being a sinusoid. This important difference suggests that the error growth of a position based navigation system which depends on ABS encoder counts is not dictated by the variance the ABS sensor quantization. Section 7.3 shows the heading error growth for test data and the error growth predicted by a white noise analysis. Section 7.2.3 confirms this by showing an encoder with 100 [ticks/rev] performs just as well as an encoder with 2000 [ticks/rev].

4 GPS & ABS WHEEL SPEEDS

Qualitatively, this estimator uses GPS heading and velocity to estimate wheel radii while the GPS signal is available and uses the wheel radii in addition to equation 3 to estimate heading while GPS is unavailable.

One way to write the equations of motion for this system is:

$$\begin{bmatrix} \dot{E} \\ \dot{N} \\ \dot{\psi} \\ R^r \\ R^l \end{bmatrix} = \begin{bmatrix} -V\sin(\psi) \\ V\cos(\psi) \\ r \\ 0 \\ 0 \end{bmatrix} \tag{19}$$

$$\triangleq f(x,t) \tag{20}$$

When GPS is available, it provides the following measurements

$$\begin{bmatrix} GPS_E \\ GPS_N \\ GPS_\psi \\ GPS_V \end{bmatrix} = \begin{bmatrix} E \\ N \\ \psi \\ V^r/2 + V^l/2 \end{bmatrix} \tag{21}$$

$$\triangleq H(x,t) \tag{22}$$

where V is the vehicle speed, ψ is the heading angle and r is the vehicle yaw rate. V^r,V^l are the right and left wheels angular velocities. R^r,R^l are the right and left wheel effective rolling radii and are modeled as slowly varying constants, their purpose in the state will become apparent shortly.

When GPS is unavailable,

$$H(x,t) = \begin{bmatrix} 0 & 0 & 0 & 0 \end{bmatrix}^T \tag{23}$$

For our system, we wish to model the vehicle speed and yaw rate as a function of the vehicle ABS sensor angle measurements. This is done by discretizing the dynamics and using the relationships developed in equation 3.

$$\hat{\Omega}^r_k = \frac{\hat{\theta}^r_k - \hat{\theta}^r_{k-1}}{\Delta t} \tag{24}$$

$$\hat{\Omega}^l_k = \frac{\hat{\theta}^l_k - \hat{\theta}^l_{k-1}}{\Delta t} \tag{25}$$

$$\hat{r}_k = \frac{\hat{\Omega}^r_k R^r - \hat{\Omega}^l_k R^l}{tw_r} \tag{26}$$

$$\hat{V}_k = \frac{\hat{\Omega}^r_k R^r + \hat{\Omega}^l_k R^l}{2} \tag{27}$$

It is clear from these equations that estimates of the wheel radii are necessary to infer velocity and heading information when GPS is unavailable.

These equations fit nicely into an EKF structure [5, 16] propagated with euler integration. At each time step,

$$h_k = \frac{\partial H}{\partial x_k(-)} \tag{28}$$

$$L_k = P_k(-)h_k^T(h_k P_k(-)h_k^T + R_k)^{-1} \tag{29}$$

$$x_k(+) = x_k(-) + L(y_k - h_k x_k(-)) \tag{30}$$

$$P_k(+) = (I - L_k h_k)P_k(-) \tag{31}$$

$$x_{k+1}(-) = x_k(+) + f_k \Delta t \tag{32}$$

$$F = \frac{\partial f_k}{\partial x_k(+)} \tag{33}$$

$$Q = Q_k \Delta t \tag{34}$$

$$P_{k+1}(-) = P_k(+) + (FP_k(+) + P_k(+)F^T + Q) * \Delta t \tag{35}$$

Where

$$\begin{aligned} L_k &= \text{Kalman gain} \\ P_k &= \text{State covariance} \\ R_k &= \text{Measurement covariance} \\ x_k &= \text{Discrete state estimate} \\ y_k &= \text{Measurement} \\ I &= \text{Identity matrix} \in \Re^{4,4} \\ \Delta t &= \text{Time step} \\ Q_k &= \text{Model covariance} \\ &= \text{diag}\begin{bmatrix} \sigma_x^2 & \sigma_y^2 & \sigma_\psi^2 & \sigma_{R_r}^2 & \sigma_{R_l}^2 \end{bmatrix} \end{aligned} \tag{36}$$

A more complete discussion of the matrices R_k and Q_k will follow in the section on filter tuning. Although omitted here, it is not difficult to show that this filter is completely observable when GPS is available and the vehicle is moving.

Estimating individual wheel radii is crucial for this filter. Differential errors in radii couple directly as

a velocity dependent bias in the yaw rate estimate. From equation 3,

$$e^H \cong \int_0^t \frac{\Omega_{ws}(\delta R^r - \delta R^l)}{tw}\, d\tau \qquad (37)$$

Where Ω_{ws} is the average wheelspeed for the rear wheels. Assuming a differential radius error of $0.001[m]$ for the wheel radius estimates and a vehicle velocity of $10[m/s]$, one would have an integrated error of $6[rad]$ in $300[sec]$ for the tests in this paper.

5 LOW COST GYRO AND GPS

This estimator uses GPS to calibrate the scale factor and bias of a commercially available MEMS gyro which is available for stability control systems. Assuming the gyro measurement has a DC bias and a scale factor error

$$\hat{r}(t) = ar(t) + b \qquad (38)$$

$$\Rightarrow r(t) = \frac{\hat{r}(t) - b}{a} \qquad (39)$$

$$\triangleq \dot{\psi}(t) \qquad (40)$$

One way to write the equations of motion for this system is:

$$\begin{bmatrix} \dot{E} \\ \dot{N} \\ \dot{\psi} \\ R^r \\ R^l \\ 1/a \\ b/a \end{bmatrix} = \begin{bmatrix} -V\sin(\psi) \\ V\cos(\psi) \\ \frac{1}{a}\hat{r} - \frac{b}{a} \\ 0 \\ 0 \\ 0 \\ 0 \end{bmatrix} \qquad (41)$$

$$\triangleq f(x,t) \qquad (42)$$

When GPS is available, the following measurements are available

$$\begin{bmatrix} GPS_E \\ GPS_N \\ GPS_\psi \\ GPS_V \\ r \end{bmatrix} = \begin{bmatrix} E \\ N \\ \psi \\ V^r/2 + V^l/2 \\ V^r/tw_r - V^l/tw_r \end{bmatrix} \qquad (43)$$

$$\triangleq H(x,t) \qquad (44)$$

When GPS is unavailable,

$$H(x,t) = \begin{bmatrix} 0 \\ 0 \\ 0 \\ 0 \\ V^r/tw_r - V^l/tw_r \end{bmatrix} \qquad (45)$$

All velocities are modeled the same as for the previous filter.

This filter structure can be interpreted as one which estimates wheel radii as well a gyro bias and scale factor when GPS measurements are available, and uses the gyro to estimate heading and the calibrated wheel radii to estimate the longitudinal distance travelled when GPS measurements are unavailable. It is not difficult to show that this filter is fully observable when GPS is available and the vehicle path has non-constant curvature.

Since the two wheel velocities are averaged to estimate the vehicle velocity, it is natural to consider using a single "equivalent" radius in place of the two independent radii. Such an approximation can be made as long as the difference between the two radii is known to be small. This can be shown by looking at the velocity at each wheel.

$$R^{eq}(t) \triangleq \frac{2V(t)}{\Omega^r + \Omega^l} \qquad (46)$$

$$= 2\left(\frac{1}{R^r} + \frac{1}{R^l} + \frac{rtw_r}{R^r} - \frac{rtw_r}{R^l}\right)^{-1} \qquad (47)$$

From the above equation, when the yaw rate is zero the equivalent radius looks like the parallel combination of the right and left wheel radii. When the two radii are identical, the yaw rate terms cancel each other out. However, when a vehicle with different right an left wheel radii is turning the equivalent radius becomes a function of the vehicle yaw rate. For a radius difference of $5[mm]$ during parking lot maneuvers at 10[m/s], the effective radius will shift by $0.15[mm]$. A vehicle travelling at $10[m/s]$ would expect a longitudinal distance error of only $0.5[m]$ for the 5 minute the data runs that appear in this paper. A radius difference of $5[cm]$, however, would generate an error of $15[m]$.

6 FILTER TUNING

As discussed above, no pre-processing of the ABS wheel angle sensors is required. Although the signals appear noisy, prefiltering the signals just adds unmodeled dynamics to the filter structure and slows down parameter convergence.

For all Kalman filters, the ratio of process uncertainty (Q_k) and sensor uncertainty (R_k) determines the final observer gains [9]. To limit the heuristics of the tuning process as much as possible, GPS sensor covariances in R_k were taken from the Novatel data sheet. The MEMS gyro covariance was experimentally determined from 15 minutes of data taken with the gyro stationary.

Measurement	Sensor	$1\ \sigma$
E	GPS	0.06 [m]
N	GPS	0.06 [m]
ψ	GPS	0.02 [rad]
V	GPS	0.02 [m/s]
r	Gyro	0.01 [rad/sec]

That left only the 5 or 7 diagonal entries of Q_k.

State	$1\ \sigma$	State	$1\ \sigma$
E	0.04 [m]	R^r	1.0×10^{-6} [m]
N	0.04 [m]	R^l	1.0×10^{-6} [m]
ψ^G	0.02 [rad]	$1/a$	5.0×10^{-4} [ ]
ψ^{WS}	0.06 [rad]	b/a	5.0×10^{-5} [rad/sec]

The covariances on E and N seem to have little effect on the filter time constants, and these values seemed to work well. The heading variance for the

gyro and wheelspeed estimated heading started at about what the gyro would be expected to produce and then increased slightly to predict the errors seen during experiments. The remaining random walk parameters for the constants were tuned to give a reasonable tradeoff between smoothness and convergence rate.

7 NAVIGATION FILTER RESULTS

7.1 Experimental Setup

All data analyzed in the following section was recorded on a 1998 Ford Windstar minivan with direct taps into the variable reluctance ABS sensors. Additional equipment includes a Novatel OEM4 GPS receiver and a Versalogic single board computer running the MATLAB XPC embedded realtime operating system. This system records and processes 20 data streams comfortably at sample rates up to 1000 hz.

Length scale can be difficult to visualize when represented as MATLAB plots. The three different test tracks used for analyzing the performance of each navigation filter appear in figure 6 for comparison. The smallest track is the top of a large parking

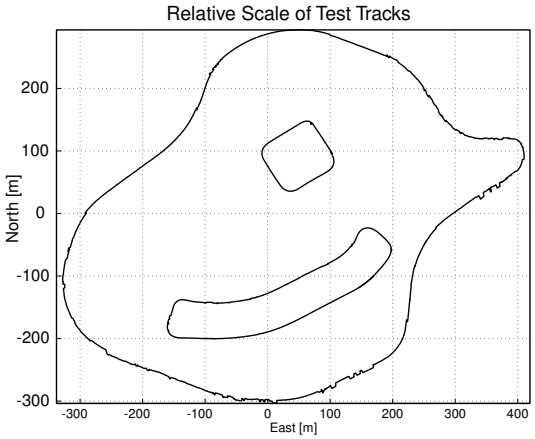

Figure 6: The relative scale of each test track

garage, the second is a large mostly flat parking lot and the third is the outer perimeter of a commercial complex. All of the maneuvers are performed at around $10[m/s]$.

For each data run a single loop of the trajectory taken from GPS measurements will be the top black trace. The lighter color traces under the top trace are the integrated position measurements. In each test the global position and heading errors are calculated by subtracting the EKF predicted position from the measured GPS position. The GPS position was taken as "truth" despite its inherent variance.

7.2 Position Estimation Results

In all six cases, the filters used the same covariance matrices R_k and Q_k defined above. Additionally, each test appearing in this paper started with the same steady state covariances generated on an alternate parking lot data run. The filters were not tuned differently for each test track.

GPS unavailability was simulated by removing the GPS signal in software near the beginning of each data run. GPS is turned back on for the last 5 seconds of each data run to illustrate the transients associated with re-gaining a GPS position solution.

7.2.1 Parking Garage

The first test site was a perfectly flat smooth parking garage with about $70[m]$ on a side. The sky is unobstructed and the route can be navigated safely using only the throttle and coasting. No braking (which would tend to slip the rear wheels) is required. This is nearly an ideal environment for the navigation filters because most of the modeling assumptions hold.

Figures 7 shows the path driven on the top of a large parking garage. Over a 230 second period, the vehicle traverses about 6 laps and $2.02[km]$.

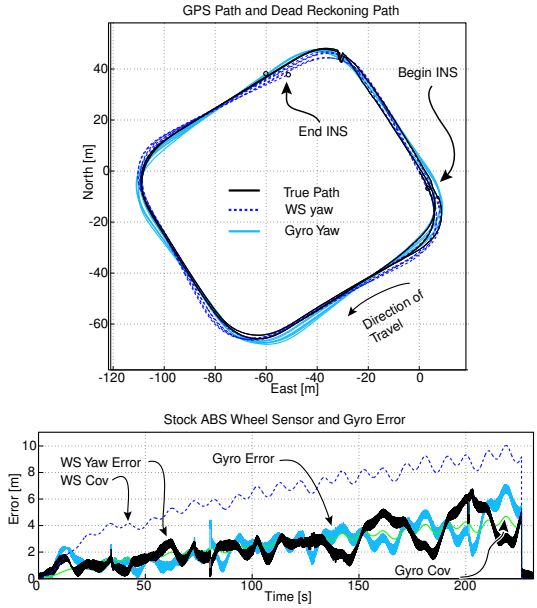

Figure 7: Wheelspeed heading Vs. gyro heading with ABS sensors

Parking Garage	ABS	Gyro
Position Error	6 $[m]$	6 $[m]$
Error Rate	$0.025[\frac{m}{s}]$	$0.025[\frac{m}{s}]$
% Error	0.3 %	0.3 %
Heading Error	0.01 $[rad]$	0.01 $[rad]$
Error Rate	$3.5e^{-4}[\frac{rad}{sec}]$	$3.5e^{-4}[\frac{rad}{sec}]$
% Error	0.25%	0.25%

The wheelspeed INS and the gyro based INS predict the position and heading equally well for these test conditions. Any dramatic jumps in the position error plot are the result of sudden jumps in the GPS position solution.

7.2.2 Longitudinal Slip

The kinematic model used for these filters assumes no longitudinal slip for the tire road interaction. Even during normal driving conditions, undriven wheels slip as a result of rolling resistance and braking. Rolling resistance for a tire stays close to

constant and thus any global velocity based identification of the effective radius will automatically account for slip. The work in this paper assumed no wheel slip during braking.

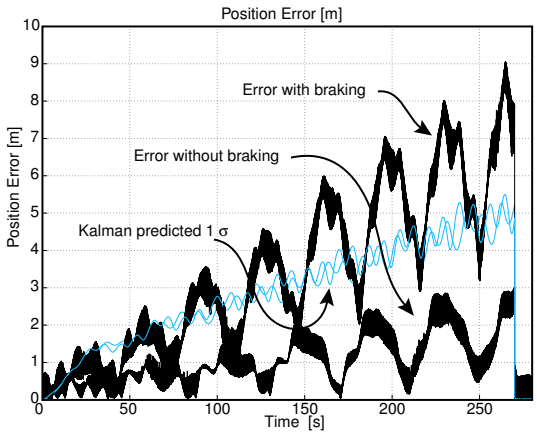

Figure 8: Error accumulation during dead-reckoning. The vehicle which uses brakes to decelerate accumulates more error than one which does not.

Figure 8 shows the global position error for two different drivers navigating the top of a parking garage. The first driver uses no brakes during the run and accumulates a global position error of about $3[m]$ in 4.5 minutes. The second driver uses the brakes to slow down before each turn and accumulates about $9[m]$ of total error in the same time period. The additional error for the second driver is probably due to low amounts of wheel slip during braking. For the low values of slip experienced during normal driving conditions, it may be possible to compensate for slip using ABS sensors and GPS [2].

7.2.3 Wide Parking Lot

This lot is larger, has very mild slopes for water runoff and occasional bumps where the surface is elevated to facilitate water runoff. This lot is less ideal as the bumps tend to excite the wheel hop dynamics and there tends to be some braking for the turns.

Wide Lot	ABS	Gyro
Position Error	31 $[m]$	8 $[m]$
Error Rate	$0.106[\frac{m}{s}]$	$0.026[\frac{m}{s}]$
% Error	1.04 %	0.27 %
Heading Error	0.07 $[rad]$	0.018 $[rad]$
Error Rate	$2.8e^{-4}[\frac{rad}{sec}]$	$7e^{-5}[\frac{rad}{sec}]$
% Error	0.4%	0.1%

As suggested in the earlier section on white noise modeling the high resolution wheel angle encoders performed identically to the ABS sensors in all data runs. Figure 9 illustrates this with dead-reckoning in the wide parking lot. The lower two plots show the error growth is independent of the wheel angle sensor used.

7.2.4 Commercial Outer Loop

The final location is the longest and the most challenging lot. It has speed bumps placed along the trajectory which will tend to excite the wheel modes. It

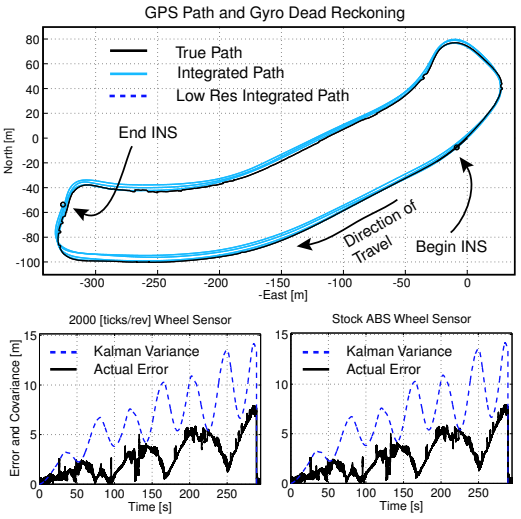

Figure 9: Integrated paths using Gyro, high resolution encoder and ABS sensors

also has a crown for water runoff and the bumps are lower on the outside of the road than on the inside. This lot is more heavily trafficked and thus the speeds are a little higher and there is more braking for the turns. It is not surprising that the performance of the filters is the worst on this section of road.

Figure 10 shows the path driven around a large parking lot. Over a 350 second period, the vehicle traverses 2 laps and $4.07[km]$.

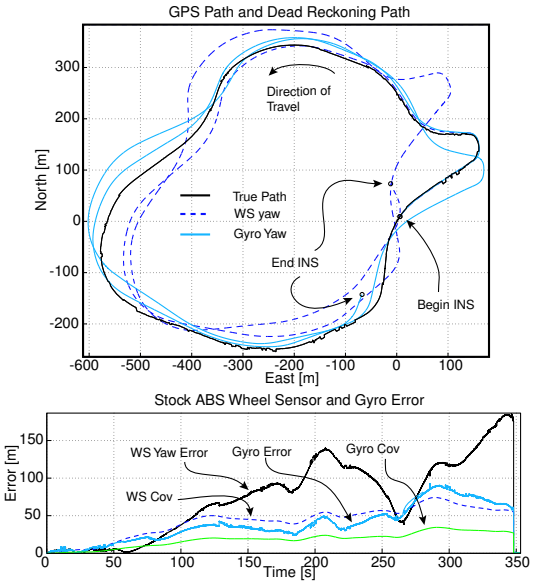

Figure 10: Wheelspeed heading Vs. gyro heading with ABS sensors

Commercial Loop	ABS	Gyro
Position Error	185 $[m]$	90 $[m]$
Error Rate	$0.53[\frac{m}{s}]$	$0.26[\frac{m}{s}]$
% Error	4.6 %	2.3 %
Heading Error	0.57 $[rad]$	0.24 $[rad]$
Error Rate	$1.6e^{-3}[\frac{rad}{sec}]$	$7e^{-4}[\frac{rad}{sec}]$
% Error	4.7%	2%

For this track the gyro navigation system does about twice as well as the wheelspeed system.

7.3 Quantization Vs. White noise

Figure 11 shows the performance of the wheelspeed heading based filters on all three parking lots. Included for comparison is the predicted 1 σ error bound for a white noise process with the same variance as the quantization errors. The error growth

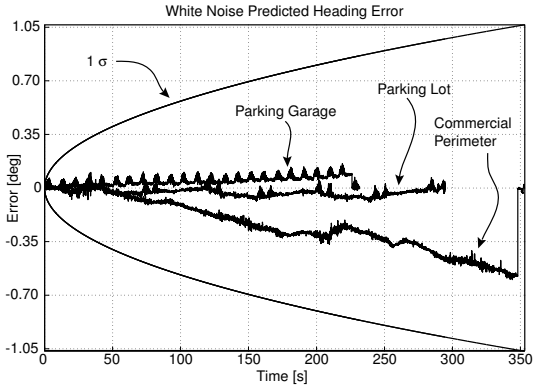

Figure 11: Actual filter performance Vs. predicted performance by modeling quantization error as white noise sequence.

for each of the heading filters is much smaller than the white noise analysis predicts. The heading errors appear to be driven by some characteristic of the test environment and not the quantization error.

8 CONCLUSIONS

Several practical aspects of vehicle navigation were considered. Navigation results show that additional encoder resolution beyond the stock ABS sensors does not aid the filter accuracy for these tests and the errors introduced by quantizing the wheel angle are not white. A kinematic analysis shows that placing the antenna over the rear differential minimizes the contribution of sideslip to the longitudinal velocity measurement. Including individual wheel radii in the filter structure is critical for the wheelspeed heading estimator and reduces the potential error sources for the gyro heading estimator when the two wheel radii differ by more than about 5$[cm]$. The gyro heading estimator appears more robust to unmodeled vehicle dynamics but may still benefit from a careful model of the tire-road interaction.

9 FUTURE WORK

The detailed sensitivity analysis in [1] purports that a dead-reckoning system can do no better than a limit set by the accuracy of the global position reference. Currently code phase correction schemes such as WAAS [4] and those outlined by the Nationwide Differential GPS [7] initiative suggest code phase corrections will be widely available in the near future. Future work will explore the performance benefits from using differentially corrected GPS position and velocity measurements.

Both estimators are sensitive to longitudinal errors due to wheel slip. Future work will explore the benefits of estimating tire longitudinal stiffness and compensating for wheel slip.

The authors would like to thank Visteon Technologies and Mahesh Chowdhary for supporting this work.

REFERENCES

[1] Eric Abbott and David Powell. Land Vehicle Navigation Using GPS. In *Proceedings of the IEEE*, volume 87, No. 1, pages 145–162, January 1999.

[2] Christopher Robert Carlson and J. Christian Gerdes. Identifying Tire Pressure Variation by Nonlinear Estimation of Longitudinal Stiffness and Effective Radius. In *Proceedings of AVEC 2002* 6^{th} *International Symposium of Advanced Vehicle Control*, 2002.

[3] David Bevly et al. The Use of GPS Based Velocity Measurements for Improved Vehicle State Estimation. In *Proceedings of the American Control Conference, Chicago IL*, pages 2538–2542, 2000.

[4] B.W. Parkinson et al. editors. *Global Positioning SystemL Theory and Applications*, volume 2. American Institute of Aeronautics and Astronautics Inc., Washington, D.C., 1996.

[5] Arthur Gelb. *Applied Optimal Estimation*. The MIT Press, Cambridge Massachusetts, 1974.

[6] J.C. Gerdes and E.J. Rossetter. A Unified Approach to Driver Assistance Systems Based on Artificial Potential Fields. In *Proceedings of the 1999 ASME IMECE, Nashville, TN.*, 1999.

[7] US Coast Guard. Nationwide Differential Global Positioning System. In *www.navcen.uscg.gov/dgps/ndgps*, 2002.

[8] Elliott D. Kaplan. *Understanding GPS*. Artech House Publishers, Boston, London, 1996.

[9] Peter S. Maybeck. *Stochastic Models, Estimation and Control. Vol 1.* Academic Press, San Francisco, 1979.

[10] Pratap Misra and Per Enge. *Global Positioning System*. Ganga-Jamuna Press, Massachusetts, 2001.

[11] R.M. Rogers. Improved Heading Using Dual Speed Sensors for Angular Rate and Odometry in Land Navigation. In *Proceedings of the Institute of Navigation National Technical Meeting*, pages 353–361, 1999.

[12] R.M. Rogers. Land Vehicle Navigation Filtering for GPS/Dead-Reckoning System. In *Proceedings of the Institute of Navigation National Technical Meeting*, pages 703–708, Jan. 1997.

[13] E.J. Rossetter and J.C. Gerdes. The Role of Handling Characteristics in Driver Assistance Systems with Environmental Interaction. In *Proceedings of the 2000 ACC, Chicago, IL*, 2000.

[14] Jihan Ryu, Eric J. Rossetter, and J. Christian Gerdes. Vehicle Sideslip and Roll Parameter Estimation Using GPS. In *Proceedings of AVEC 2002* 6^{th} *International Symposium of Advanced Vehicle Control*, 2002.

[15] M. L. Schwall and J. C. Gerdes. A Probabilistic Approach to Residual Processing for Vehicle Fault Detection. In *Proceedings of the American Controls Conference*, 2002.

[16] Robert F. Stengel. *Optimal Control and Estimation*. Dover Publications, New York, 1986.

[17] J. Stephen and G. Lachapelle. Development and Testing of a GPS-Augmented Multi-Sensor Vehicle Navigation System. *The Journal of Navigation, Royal Institute of Navigation,*, 54, no. 2(May issue):297–319, 2001.

[18] A. van Zanten et al. Vehicle Stabilization by the Vehicle Dynamics Control System ESP. In *Proceedings of the* 1^{st} *IFAC conference on Mechatronic Systems, Darmstady, Germany*, pages 95–102, 2000.